Global Research journal of Natural Science and Technology (Grjnst)

Volume: 03 - Issue 3 (2025)

p.ISSN: 2790-7643 e.ISSN: 2790-7651

High-Efficiency Chromium (VI) Removal from Contaminated Water Using Laboratory-Synthesized Nano-Ferrihydrite

Muhammad Sufhan Tahir

Institute of Soil and environmental science, University of Agriculture Faisalabad

Corresponding Author: Sufhantahir786@gmail.com

Ali Raza Khan

Gomal University of Dera Ismail Khan

raza.a46014@gmail.com

Aftab Alam

Department of Chemistry, University of Kohat University of Science and Technology

Aftabchemist.ino@gmail.com

Nadeem Jan

Department of Chemistry, Beijing University of Chemical Technology

nadeembaloch75@gmail.com

Amir Arshad

Department of Food Science and Technology, Riphah International University Faisalabad

amir.arshad@riphahfsd.edu.pk

Qaiser Ali Sultan

Pakistan Standards and Quality Control Authority, Peshawar, KPK, Pakistan

nakhuda@aup.edu.pk

Dr Farrukh Bashir

Sardar Bahadur Khan Women's University, Quetta-87300

farrukh_chem@yahoo.com

Muhammad Akash Khan

Department of Science and Engineering, University of Ryukyus

ak7367679@gmail.com

Noman Basheer

Institute of Soil and environmental science, University of Agriculture Faisalabad

Noumanbaloch266@gmail.com

Muhammad Shoaib

Department of chemistry, Islamia college university Peshawar

shoaibkundi9777@gmail.com

Mohammad Aslam

Department of Soil Science, University College of Dera Murad Jamali (LUAWMS)

m.aslam@ucdmj.luawms.edu.pk

Abstract

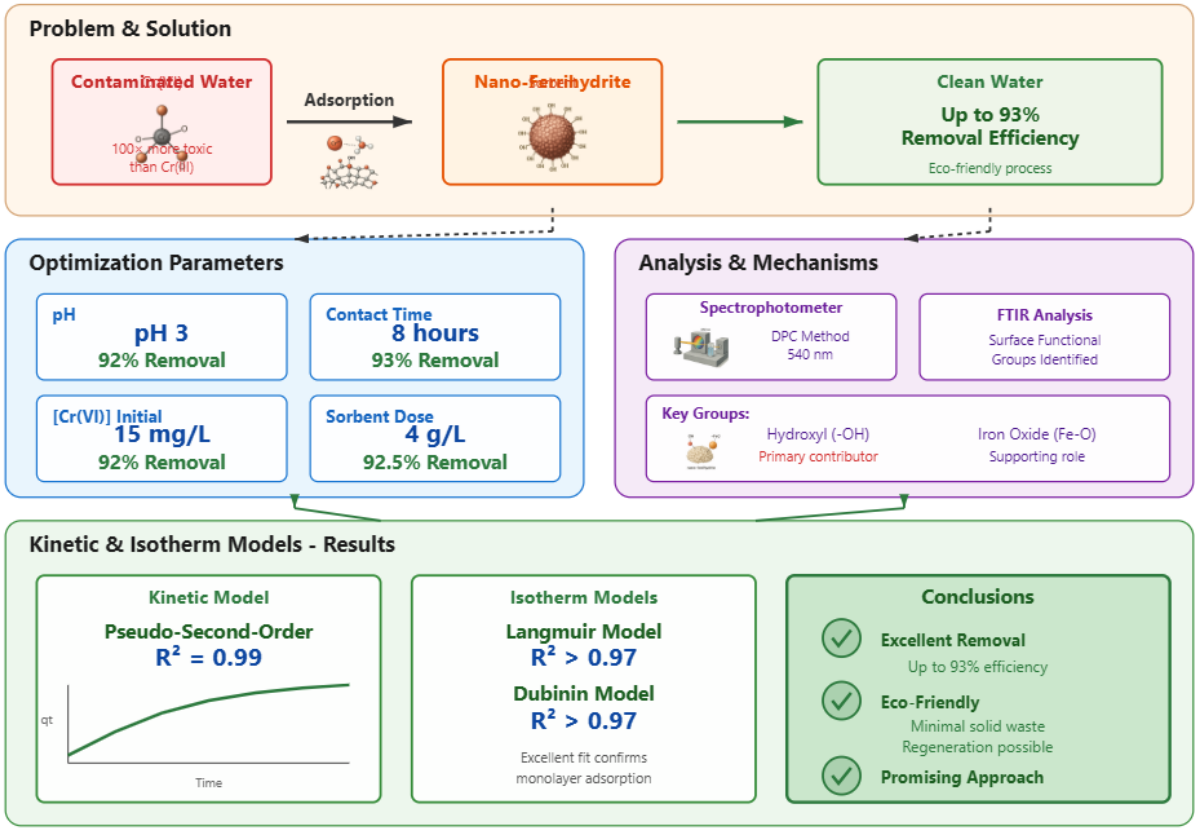

Chromium (Cr) is one of the 16th most determined toxic heavy metals globally, with hexavalent chromium (Cr(VI)) being 100 times more toxic than its trivalent form (Cr(III)) due to its better solubility and mobility in water. As a result of industrial activities, Cr is released into the environment, which poses a significant threat to human health. Therefore, this study examined the efficacy of laboratory-synthesized nano-ferrihydrite for eliminating Cr(VI) from contaminated water in relation to initial Cr(VI) concentration, contact time, pH and sorbent dose. The absorption of Cr(VI) was analyzed using the 1,5-diphenylcarbazide (DPC) method using a spectrophotometer at 540 nm wavelength. Batch sorption experiments revealed that the highest sorption capacity occurred at pH 3, achieving a sorption rate of 92%. At 8 hours of contact time, maximum sorption with a 93% removal rate was observed. At a Cr(VI) concentration of 15 mg L^{-1}, the highest sorption efficiency remained 92%. Additionally, an optimal sorbent dosage of 4 g L^{-1} resulted in a maximum sorption efficiency of 92.5%. Kinetic modeling supported the pseudo-second-order model (R^2 = 0.99), while the isothermal data fit well with the Langmuir and Dubinin models (R^2 > 0.97). Analysis by Fourier Transform Infrared Spectroscopy (FTIR) highlighted involvement of hydroxyl and iron oxide surface functional groups, with hydroxyl groups primarily contributing to chromate adsorption. Moreover, the eco-friendliness of the sorption process, which produces minimal solid waste and enables

regeneration, makes it a promising approach for Cr(VI) removal. This sorption study concluded that nano-ferrihydrite had excellent removal efficiency for Cr(VI) from contaminated water.

Keywords: *Chromium(VI), Nano-ferrihydrite, Water contamination, Sorption kinetics, Isotherm modeling, Eco-friendly remediation*

1. Introduction

Heavy metal pollution has persisted as a critical environmental problem over the past fifty years, which affects water quality and aquatic organisms (Liu *et al*., 2020). The ingestion of heavy metal-contaminated water leads to millions of illnesses affecting people across the globe. The sustainable management of water represents a crucial necessity because it equally sustains living things and acts as an important natural resource (Di Baldassarre *et al*., 2019). The rapid growth of populations, urbanization, and industrialization has placed excessive pressure on the world's water resources. Pakistani people receive safe drinking water, only 20%, as per Perveen (2023). Industrial waste discharge, specifically untreated wastewater, has led to exceptional growth of both organic and inorganic pollutants throughout river systems and lakes, as well as coastal environments (Barletta *et al*., 2019). Among these pollutants, a wide range of non-biodegradable pollutants affects both ecological system stability and seafood safety after entering or accumulating in the food chain (Almeida *et al*., 2019). Heavy metals are derived from natural processes that include sea spray emissions, volcanic activities, rock weathering, biogenic emissions and wind-borne dust (Masindi and Muedi, 2018; Nieder *et al*., 2018). These metals within the earth's crust exist as chemical ores and maintain a persistent status, thus impossible to completely remove them (Lin *et al*., 2022). Among heavy metals, the essential elements include copper (Cu) and cobalt (Co) and zinc (Zn) that support biological functions in normal conditions. However, high metal concentration, specifically cadmium (Cd), chromium (Cr), and lead (Pb), proves toxic for human beings and aquatic organisms, although some metals, including Zn, Cu, and Co, have vital biological functions (Zoroddu *et al*., 2019; Jan et al., 2025). Globally, researchers show significant concern regarding Cr contamination because it exhibits toxic effects and causes cancer, according to Ahmed *et al*. (2019) and Zhao *et al*. (2019).

The metallic form of Cr exists in two main forms: The Cr(III) and the Cr(VI). The human body uses Cr(III) as a trace element to support lipid and glucose metabolism (Liu *et al*., 2020), but Cr(VI) exists as an extremely toxic mutagenic substance with carcinogenic properties. The oxidizing conditions within aqueous environments support Cr(VI) to exist as highly soluble, mobile chromate (CrO_4^{2-}) and dichromate ($Cr_2O_7^{2-}$) species (Zhou *et al*., 2016). Because Cr (VI) can penetrate biological membranes and damage cells, it is 100 times more hazardous than Cr (III). However, Cr(VI) is reduced to the less toxic Cr(III) when environmental conditions become

reducing (Kapoor *et al*., 2015). Due to its hazardous nature, the enforcement bodies have established strict regulations regarding Cr content found in water systems. According to the United States Environmental Defense Agency (USEPA), the maximum total Cr is 0.1 mg/L in drinking water and 0.015 mg/L in surface water (Bagbi *et al*., 2017; Jan et al., 2025). As one of ten hazardous chemicals according to Georgaki *et al*. (2023), Cr(VI) faces regulatory requirements that establish a maximum drinking water threshold of 0.05 mg L^{-1} total Cr. On the other hand, Zhou *et al* (2016) noted that industrial effluent contains Cr(VI) between 30 and 200 mg L^{-1}. The elevated concentration is due to industrial processes that utilize Cr extensively, such as electroplating, leather tanning, steel manufacturing, mining, paper production, dyeing, and wood preservation (Dzieniszewska *et al*., 2020). In particular, the production of stainless steel that contains 12-15% Cr depends on ferrochromium to achieve corrosion resistance, according to Xu *et al*. (2023). The worldwide production of Cr containing wastewater reaches approximately 40 million tons each year from tannery industries (Jobby *et al*., 2018). Exposure to Cr, particularly Cr (VI), causes severe health complications that lead to liver and kidney failure, anemia, allergic reactions, asthma and develop into cancers of the lungs and digestive tract (Liu *et al*., 2020).

The uncontrolled release of toxic substances occurs in developing nations due to a lack of sufficient infrastructure, while developed countries treat industrial waste before disposal (Hassan and Saleh, 2022). In particular, Pakistan deals with major issues regarding heavy metal contamination, mainly focused on Cr contamination (Afzaal *et al*., 2022; Jan et al., 2025). Researchers have applied various treatment methods (Figure 1), which remove Cr (VI) from polluted water through oxidation-reduction adsorption, membrane separation, chemical precipitation, reverse osmosis, ion conversion and ultrafiltration (Kong *et al*., 2016; Itankar and Patil, 2022). Among these, the method of adsorption stands out as an effective and cost-efficient treatment due to its simple operational principle and selective capacity, as well as high removal efficiency according to Zhou *et al*. (2016). Sorption functions as a physicochemical method that

incorporates a sorbent solid material to extract contaminants from both liquid and gaseous phases (Al-Sabagh *et al*., 2018; Yusuff, 2019).

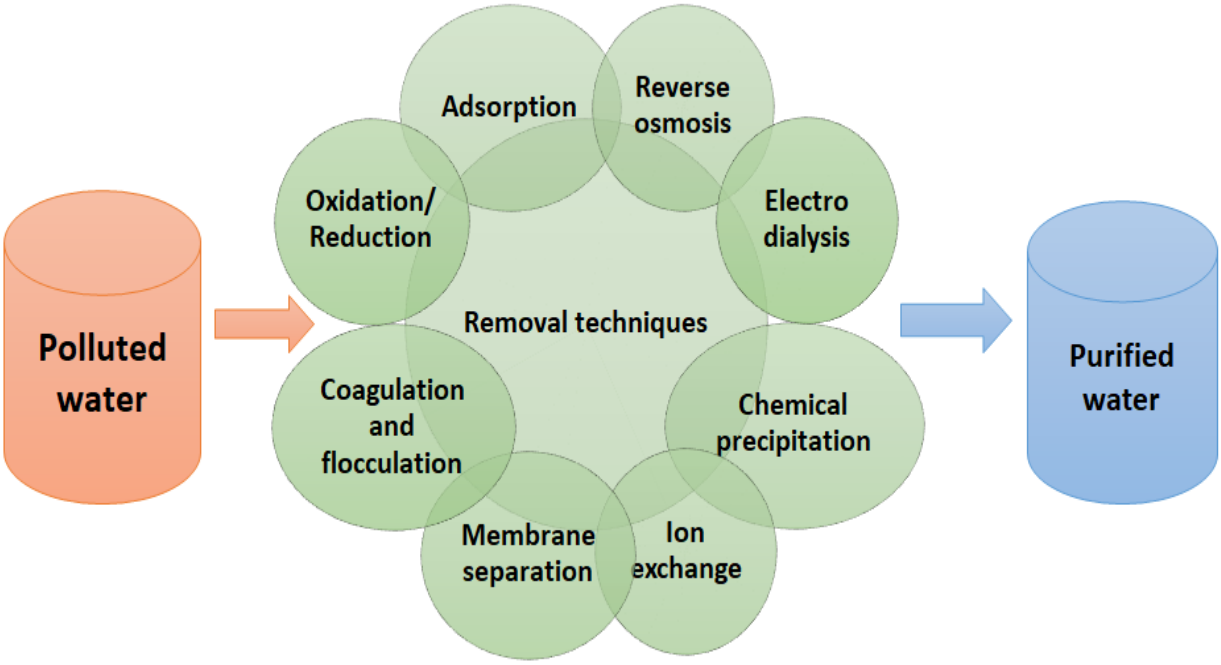

Figure 1: Remediation techniques for water treatment

Research on adsorbents for Cr(VI) removal focuses on materials such as pyrite fines, synthetic polymers, activated carbon, graphene oxide and manganese-oxide-coated sand. The combination of large surface area and low solubility and high reactivity makes iron oxides a leading sorbent among adsorption materials (Shi *et al*., 2015; Dzieniszewska *et al*., 2020). Significant forms of iron oxides include magnetite (Fe_3O_4), hematite (α-Fe_2O_3) and maghemite (γ-Fe_2O_3) (Jerin *et al*., 2019). Metal adsorption processes utilize ferrihydrite as the amorphous iron oxyhydroxide because of its superior efficiency (Pakade *et al*., 2019). This material effectively takes up various Cr forms across natural water pH ranges. However, the transformation of ferrihydrite into hematite and goethite occurs gradually because this material displays thermodynamic instability (Zhang *et al*., 2022; Jan et al., 2025). Under acidic conditions, Cr(VI) attaches to ferrihydrite through electrostatic attraction, but this attraction weakens when the solution reaches pH of 11 (Cismasu *et al*., 2018). While the occurrence of ferrihydrite in natural soil, its complex mineral structure makes it difficult to isolate (Hiemstra *et al*., 2024). Therefore, for water treatment, synthetic ferrihydrite is used as an effective solution. This study aimed to: (1) synthesize and characterize the nano-ferrihydrite in the laboratory to evaluate its efficiency in removing Cr(VI) polluted water, (2). The influence of various factors initial Cr(VI) concentration, pH, sorbent dosage, and contact time, on the removal efficiency of the sorbent,

(3) conduct kinetic and thermodynamic modeling of the sorption data to understand the rate and mechanism of the adsorption processes, and perform FTIR analysis to confirm the sorption.

2. Materials and methods

This study was conducted in the laboratory of the Institute of Soil and Environmental Sciences (ISES), University of Agriculture, Faisalabad (UAF), Pakistan.

2.1. Chemicals and reagents

Reagents used in the batch sorption studies were analytically evaluated (Hu *et al*., 2015). Distilled water (ultrapure water) was used for all sorption trials and standard solutions. The standard stock solutions of Cr(VI) (1000 mg L^{-1}) were prepared by dissolving 5.65 g of potassium dichromate ($K_2Cr_2O_7$). For batch sorption experiments, sub-stock solutions with varying Cr(VI) concentrations were also prepared from a stock solution (Hosseini and Pasikhani, 2019). All experiments were conducted in duplicate. Throughout the experiment, the plastic and glassware were washed out with 2% nitric acid (HNO_3) and then washed twice with distilled water (DeFilippi, 2018).

2.2. Determination of Cr(VI)

To make the 0.5% DPC solution, 0.25 g of DPC was dissolved in 50 mL of acetone. The spectrophotometer was standardized by preparing standards of Cr(VI) from a Cr stock solution in the following range: 0, 0.5, 1, 2, 3, 4 and 5 mg L^{-1}. Five mL of Cr-containing samples were pipetted into 10 mL test tubes. The samples were diluted, in which the concentrations were high. The 0.1 mg L^{-1} of 2.5 M sulphuric acid (H_2SO_4) was added to each standard and samples were followed by 0.1 mg L^{-1} of 0.5% DPC solution. The lids were put on the samples and standards, which were incubated for 5 minutes. Chromium(VI) absorbance was measured on a spectrophotometer at 540 nm (Lace *et al*., 2019).

2.3. Sorbent preparation and its characterization

2.3.1. Synthesis of nano-ferrihydrite

The nano-ferrihydrite mineral was synthesized by: i) dissolving 40 g of iron nitrate ($Fe(NO_3)_3.9H_2O$) in 500 mL of purified water in a beaker, ii) adding 330 mL of 1M sodium hydroxide (NaOH) dropwise into the beaker, resulting in the formation of iron hydroxide precipitates. The precipitated solution was then centrifuged, allowed to settle overnight, and then oven-dried at 60°C for 6 hours. After attaining 60°C, the temperature was kept constant until the drying was completed (Abuzarova and Korchuganova, 2008). Figure 2 shows a schematic process of nano-ferrihydrite preparation. The synthesized mineral was packed in a plastic bag and placed

in a desiccator to prevent moisture absorption for further usage. For its use as a sorbent, the prepared product was ground to obtain the homogenized material.

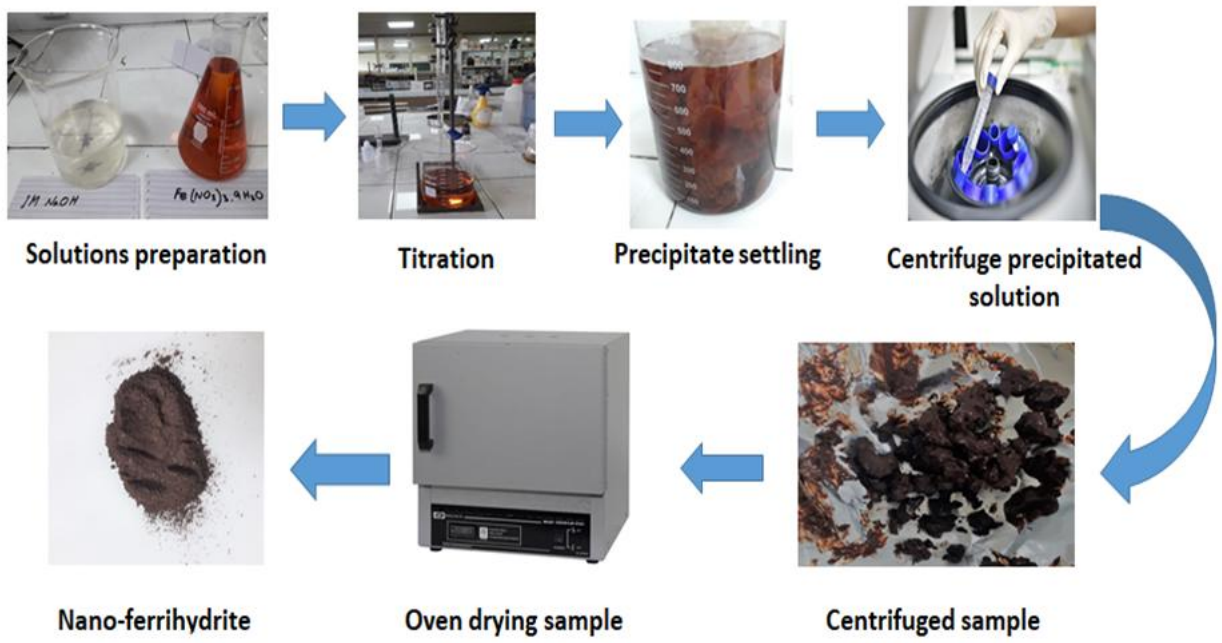

Figure 2: Process of Nano-Ferrihydrite synthesis

2.3.2. Characterization of nano-ferrihydrite

Surface functional groups of sorbent, both with and without Cr(VI) contamination involved in sorption, were characterized by FTIR (Alpha II, Bruker, Germany) spectroscopy. In FTIR, major functional groups observed on an interferogram are inferred dependent on their vibrational peaks' location. IR ranges are interpreted based on the reference spectra from preceding studies (Ochie *et al*., 2025).

2.4. Batch sorption experiments

In each batch sorption experiment, a sorbent was added to a 50 mL centrifuge tube containing the chromium solution. The equilibrium time (2 hours) was calculated according to the experimental data of the kinetics and the temperature was maintained at 25±2°C (Molavi *et al*., 2020). The effect of solution pH in the range of 2 to 10 on the sorbent surface charge at 15 mg L^{-1} initial Cr(VI) concentration and 2 g L^{-1} sorbent dose was studied. Suspension pH was maintained with either 0.1 M hydrochloric acid (HCL) or 0.1 M sodium hydroxide (NaOH) to remove Cr(VI) from contaminated water by nano-ferrihydrite. For kinetic investigations, the capacity for sorption of the sorbent was determined at various intervals of time (0, 1, 2, 3, 4, 8, 12 and 24 hours) to observe the impact of contact duration at 15 mg L^{-1} Cr(VI) concentration and 2 g L^{-1} sorbent dose. Sorption

isotherm tests were carried out using a fixed dose of sorbent (2 g L−1) and different initial concentrations of Cr(VI) (1, 5, 10, 15, and 20 mg L−1), these concentrations were selected based on monitoring of low and high concentrations of Cr(VI) in the aqueous environment contaminated with Cr(VI) (Borna *et al*., 2016). The sorbent dose efficiency was measured at different sorbent levels (0.5, 1, 2, 3, 4 g L^{-1}) with the initial Cr(VI) concentration of 15 mg L^{-1} and at pH 7. Except for contact time, all studies involved shaking the suspensions in an end-to-end shaker for two hours. The suspensions were shaken and then centrifuged for three minutes at 3000 rpm. This caused the solid residue to separate from the solution of supernatant. A 0.45 μm filtration film was then used to filter the solution. Filtered samples were stored at 4°C for analysis after calculating the equilibrium pH of the solution.

The amount of Cr(VI) removed from the solution was calculated using this equation.

$$\% \, Cr \, removal = \frac{C_o - C_e}{C_o \times 100} \times 100$$

In the formula above, Co stands for the initial concentration of Cr(VI) in solutions (mg L^{-1}) and Ce for the ultimate concentration of Cr(VI) in solution (mg L^{-1}). The following formula was used to determine the sorption capacity (qe) at equilibrium.

$$q_e = \frac{(C_o - C_e)\, V}{m}$$

Where m is the oven-dried sorbent weight (g), and V is the volume of solution (l) (Masood ul Hassan et al., 2023).

2.5. Modeling

Kinetic modeling (pseudo first-order and pseudo second-order) and isotherm equilibrium modeling (Langmuir, Freundlich, Temkin and Dubinin-Radushkevich) were performed using the Sigmaplot 10® software and Microsoft Excel.

3. Results and discussion

3.1. Impact of pH on Cr(VI) sorption

Nano-ferrihydrite efficiently removed Cr(VI) contaminants, with removal effectiveness strongly dependent on solution pH. The Cr(VI) adsorption rate displayed an inverse relationship with pH variation, resulting in lower removal efficiency as pH increased (Figure 3). The optimum sorption occurred at pH 3, where Cr(VI) removal reached 92%, but a lower sorption of 88% occurred at pH 10. This study demonstrates that nano-ferrihydrite achieves superior Cr(VI) removal under acidic

conditions, as the elevated amounts of hydrogen ions (H^+) at lower pH levels result in surface protonation of nano-ferrihydrite, which generates positively charged sites. These positive surface charges increase electrostatic interactions for the most dominant Cr(VI) species, $HCrO_4^-$, in acidic solution, therefore increasing adsorption efficiency. The excess H^+ ions reduce the inhibitory effect of hydroxide ions (OH^-) on adsorption because they attract the negative chromate ion charge more effectively in this environment (Liang *et al*., 2023). Variations in pH affect the ionization state of the sorbate and the sorbent surface charge properties, which are critical elements for metal adsorption, while also changing the speciation of Cr(VI) (Kucic *et al*., 2017). This study examined Cr(VI) removal across the pH values from 2 to 10 for a complete assessment of its removal effects. Increases in pH value generate OH^- that compete against chromate anions to occupy adsorption sites. Electrostatic repulsion occurs between Cr(VI) species and the sorbent surface because their deprotonation increases their surface negative charge. This interaction reduces the removal effectiveness by blocking the adsorption process (Fenti *et al*., 2020).

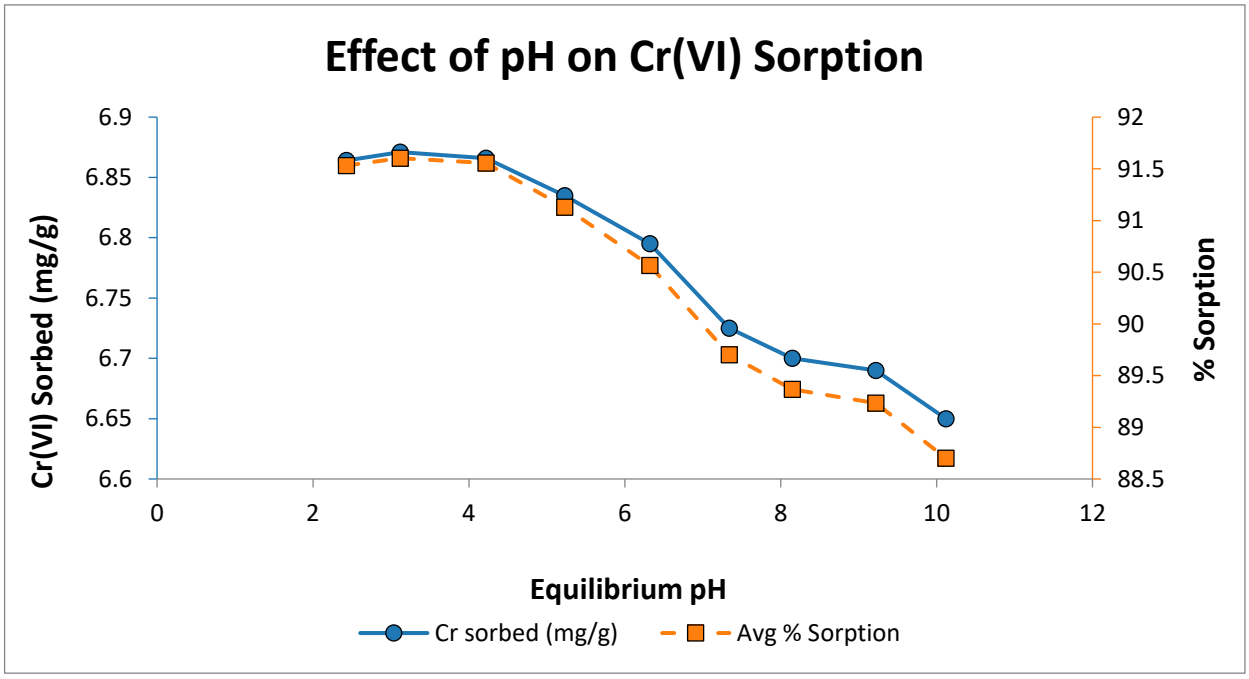

Figure 3: Effect of pH (3–10) on the sorption of Cr(VI) using nano-ferrihydrite at a concentration of 15 mg L^{-1} and a sorbent dosage of 2 gL^{-1}

3.2. Effect of reaction duration on Cr(VI) sorption

Water treatment requires a thorough investigation of equilibrium time and uptake rate because such factors directly influence operational economics (Wang *et al*., 2023). The contact duration for Cr(VI) sorption on nano-ferrihydrite was determined by analyzing various contact times (1, 2, 3, 4, 8, 12, 24) until equilibrium was reached. Figure 4 illustrates the nano-ferrihydrite efficiency

for removing Cr(VI) as the contact time duration is varied. Early in the sorption process, there were many sorption sites available, which allowed for the rapid removal of Cr(VI) up to 4 hours of contact time. As the interaction time increased, surface site saturation caused CrVI) ions to compete with one another for sorption sites, which decreased sorption (Binabaj *et al*., 2018; Chen *et al*., 2018). Maximum sorption occurred at 8 hours, which was 93% and minimum sorption occurred at 1 hour, which was 84%. The data shows that sorption increases over time toward equilibrium, which is finally reached at 8 hours of contact duration. The equilibrium time is primarily dependent on the nature of the adsorbent, compactness, and other properties (Shin *et al*., 2024). The study of Ali *et al*. (2019) established that 100 min and 120 min marked the complete attainment of the Cr(VI) sorption rate, while an increase in contact time showed no impact on metal removal.

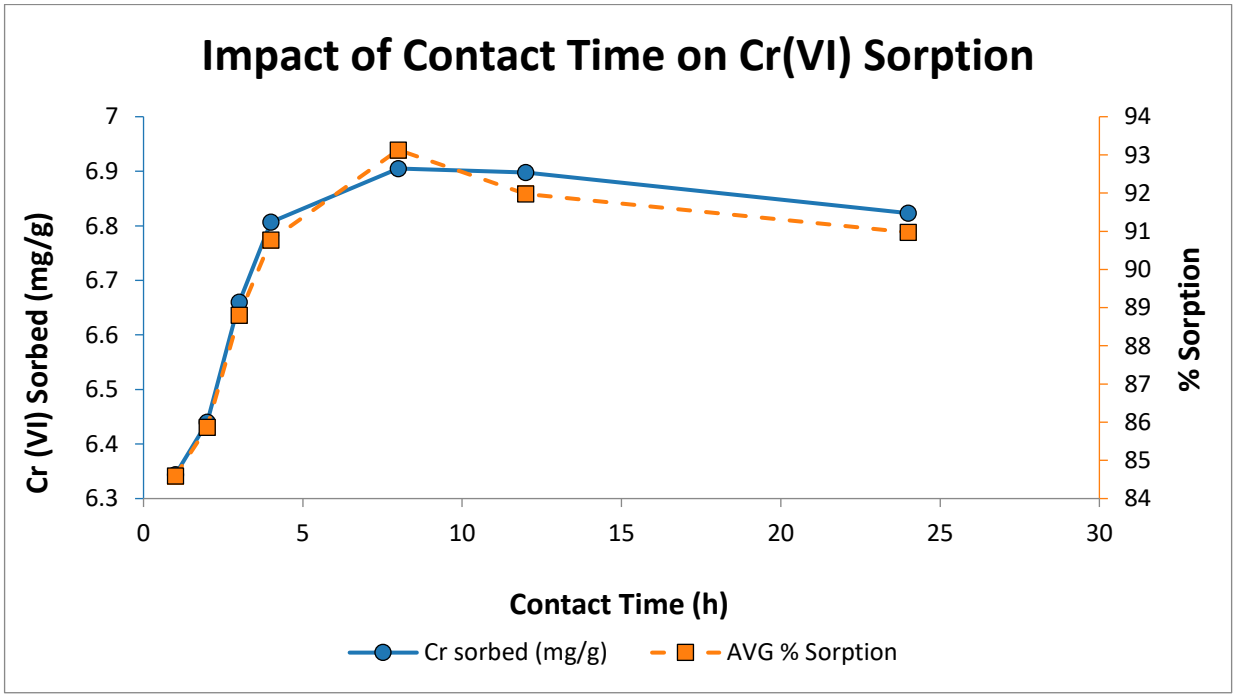

Figure 4: Impact of contact time (1-24 hours) on Cr(VI) sorption via nanoferrihydrite at a Cr(VI) concentration of 15 mgL^{-1} and a sorbent dosage of 2 gL^{-1}

3.2. Impact of initial Cr(VI) concentration changes on Cr sorption

Two-hour contact reaction between nano-ferrihydrite and Cr(VI) ions at pH of 7 was used to measure sorption capacity across a range of initial Cr(VI) concentrations from 1-20 mg L^{-1}. Figure 5 illustrates that the sorption of Cr(VI) by nano-ferrihydrite increased rapidly from 76.1 to 91.22 % as the equilibrium Cr(VI) concentration rose from 0.2 to 1.8 mg L^{-1}. An increase in initial adsorbate concentration strengthened the driving energy needed to overcome all metal ion transfer resistances between solid and aqueous phases, allowing Cr(VI) ions to interact with

available active sites; therefore, initial Cr(VI) concentration significantly affects sorption processes (Shyaa *et al*., 2015). The number of available sorption sites was scarce, and the initial Cr(VI) ion concentration was low; however, increasing this concentration strengthened the bond between Cr(VI) ions and sorption sites until equilibrium was achieved (Khalil *et al*., 2020). The Cr(VI) uptake increased as initial concentrations of Cr(VI) rose, but only reached a limit because the sorbent dose and active sites remained constant. Nano-ferrihydrite exhibits a larger surface area available for the 1 mgL^{-1} of the initial Cr(VI) concentration, while the available surface area decreases with increasing concentration of Cr(VI), resulting decrease in removal efficiency as reported by Owalude and Tella (2016). The study also demonstrated that increased Cr(VI) concentration led to higher adsorption capacity; however, no direct correlation was found between Cr(VI) concentration and adsorption capacity (Islam *et al*., 2019).

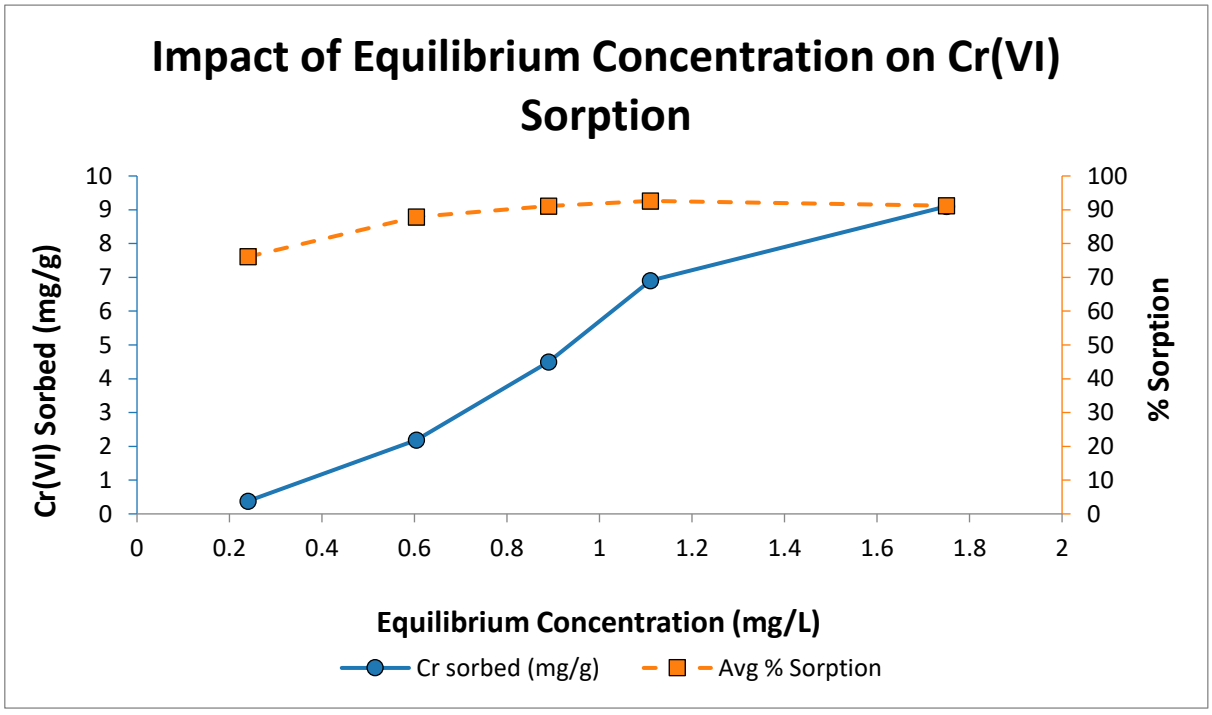

Figure 5: Effect of equilibrium Cr(VI) concentration (0.24 – 1.7 mg L^{-1}) on sorption of Cr(VI) by nano ferrihydrite

3.3. Sorbent dosage effect on sorption of Cr(VI)

Investigated the effects of sorbent doses ranging from 0.5 to 4 g L^{-1} on the removal of Cr(VI) utilizing an initial concentration of 15 mg L^{-1} of Cr(VI) at pH 7 and a 2-hour contact duration. As the amount of sorbent increased, the sorption of Cr(VI) also enhanced; however, an overabundance of sorbent led to insufficient use of surface-active sites, which also increased expenses and resource waste (Baskar *et al*., 2022). Figure 6 shows that the maximum sorption of 92% occurred with the adsorbent dosage of 4 g L^{-1}, while the minimum sorption of 86% happened with the

sorbent dosage of 0.5 g L^{-1}. The high sorbent dose would also reduce Cr(VI) sorption due to sorbent particle overcrowding and sorption site overlapping (Kokab *et al*., 2021). On the other hand, as the sorbent dose increased, the quantity of transferrable and superficial sites designated for Cr(VI) sorption also increased (Fenti *et al*., 2020). However, with further increased nano-ferrihydrite dose, no substantial changes in Cr adsorption occurred. This can be because of the lower concentrations of the metal and the higher availability of the sorption sites and the reaction has already reached equilibrium. The adsorption reaches its maximum capacity point at a specified adsorbent dose since the ion binding to the adsorbent matches the amount of free ions, despite additional adsorbent usage (Chakraborty *et al*., 2022). The effectiveness of Cr(VI) adsorption declined as the amount of the sorbent rose because the effective surface area diminished, and the adsorbate/adsorbent ratio became smaller (Alsuhaibani *et al*., 2024). Although the reduction of adsorption density occurs because several absorption sites fail to get saturated during adsorption; however, additional adsorption sites become available as adsorbent concentrations rise, thus leading to enhanced removal efficiency (Zhang *et al*., 2022).

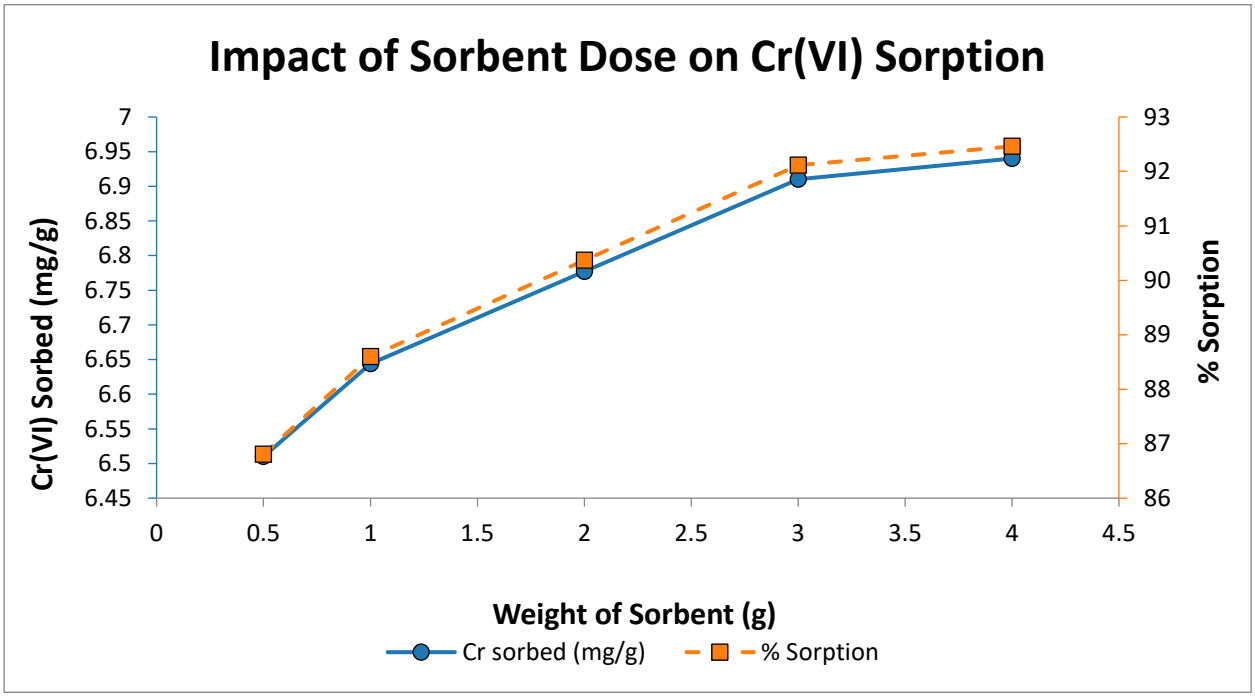

Figure 6: Effect of sorbent dose (0.5 to 4 gL^{-1}) on the Cr(VI) sorption by nanoferrihydrite. Experimental setup: initial Cr(VI) concentration 15 mg L^{-1}, contact time 2 hours.

3.4. Kinetic modeling

The adsorption efficiency of chromate anions on the nano-ferrihydrite in terms of kinetic studies needs to be defined. These investigations aid in analyzing the system's adsorption capability as well as the kind of adsorption that takes place. A pseudo-first-order model explains the adsorption

potential of a solid sorbent. When this model fits well with data, which shows a physical adsorption process and the model equation is as follows (Tiadi *et al*., 2017).

$$\text{Log}(q_e - q_t) = \frac{\log q_e - k_1 t}{2.303}$$

Where q_t is the sorbed Cr(VI) at any time t (mg g-1), q_e is the sorbed Cr(VI) (mg g-1), and k_1 is the rate constant of equation (min^{-1}). By plotting log $(q_e - q_t)/t$, k_1 can be calculated experimentally. The pseudo-second-order model shows that the degree of adsorption is proportional to the square of the remaining free sorption sites. If it fits well with the data, showing a chemical sorption process and the model equation is given below (Wang *et al*., 2019).

$$\frac{t}{q_t} = \frac{1}{k_2 q^2 e} + \frac{t}{q_e}$$

In the equation above, k_2 represents the equilibrium sorption rate constant (g mg^{-1} min-1). An intercept of $1/(k_2 q^2 e)$ and a slope of $1/q_e$ indicate a linear relationship between t/qt and t. The linear relation further showed that sorption depended on both the quantity of Cr(VI) previously adsorbed and site availability (Chakraborty *et al*., 2021). Therefore, it can be said that the pseudo-second-order model provides an extra precise explanation of Cr(VI) sorption and raises the possibility that the sorption process is rate-limiting (Cao *et al*., 2021).

Figure 7 and Table 1 display the variables of the kinetic model derived from the pseudo-first and second-order models. As compared to the pseudo-first-order model ($R^2 = 0.18$), the results showed that the pseudo-second-order model determination coefficient value ($R^2 = 0.99$) is greater. Furthermore, q_e value derived from the pseudo-first and second-order model was near to similar. Based on kinetic modeling data with a higher R^2 and qe, the pseudo-second-order fits well with data and describes the chemisorption of Cr(VI). During the process of chemisorption, the formation of chemical bonds between the nano-ferrihydrite surface and Cr(VI) ions takes place. In addition, pseudo-first-order model shows that rapid sorption takes place during the early stages. Thus, it indicates that a strong trigger of Cr(VI) ions was made to occupy available sorption sites. As a result, fast Cr(VI) sorption is observed and the adsorption rate decreases as sorption sites are occupied. This shows that initial rate of adsorption was regulated by availability of active sites (Liu *et al*., 2019).

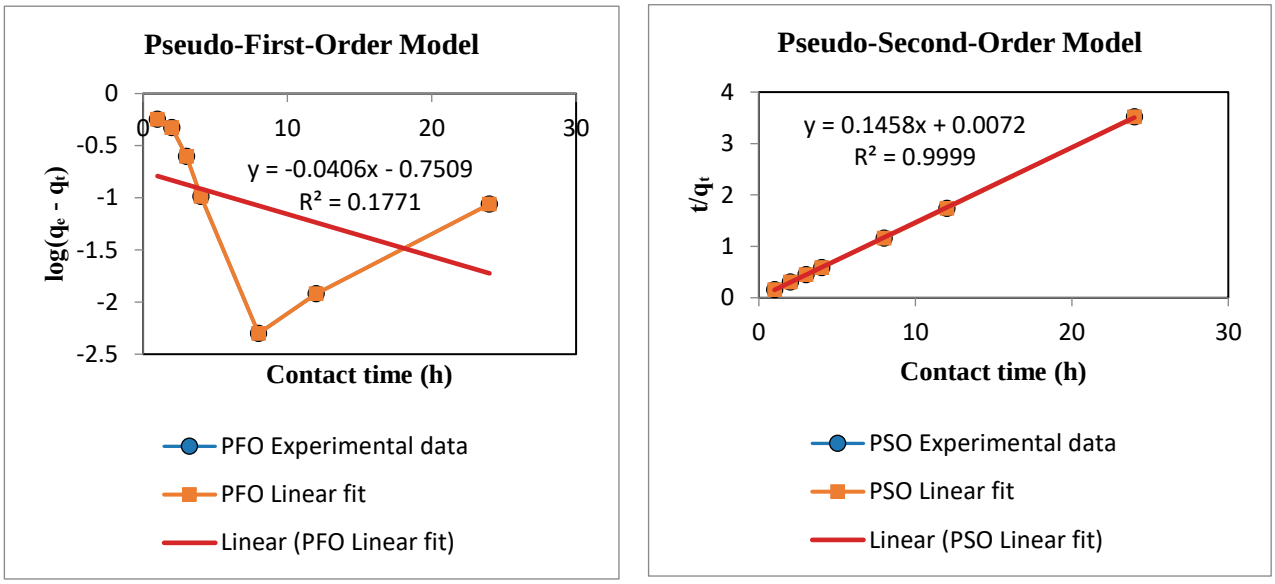

Figure 7: Plots linearized for the kinetic pseudo-first and second order models of nano-ferrihydrite-mediated Cr(VI) sorption.

Table 1: Kinetics non-linear variables for a pseudo-first and second-order models: Cr(VI) sorption to nano-ferrihydrite at a temperature of 25 °C, initial Cr(VI) concentrations ranging from 0 to 20 mg L^{-1}, and a sorbent dosage of 2 g L^{-1}.

Sorbent	**Pseudo-first-order model**			**Pseudo-second-order model**		
	qe (mg g^{-1})	**k1 (min^{-1})**	**R^2**	**qe (mg g^{-1})**	**k2 (g mg^{-1} min^{-1})**	**R^2**
Nano-ferrihydrite	4.57	0.036	0.18	6.86	0.146	0.99

3.5.Sorption isotherm

Sorption capacity, surface characteristics, and affinity of an adsorbent can be determined by adsorption isotherms (Tafakori *et al.*, 2017). The equilibrium of the Cr(VI) sorption process can be studied by utilizing two-parameter equilibrium sorption isotherm models such as the Langmuir, Freundlich, Temkin and Dubinin–Radushkevich (Ragadhita and Nandiyanto 2022). Residual plot of models confirms that the Langmuir model and Dubinin-Radushkevich model had the least deviations between the experimental and predicted values (Figure 8). The results given in Figure 9 and Table 2 showed that Langmuir and Dubinin models were found to fit better against experimental isotherm data than the Freundlich and Temkin models, as demonstrated by a greater R^2 (0.97) value.

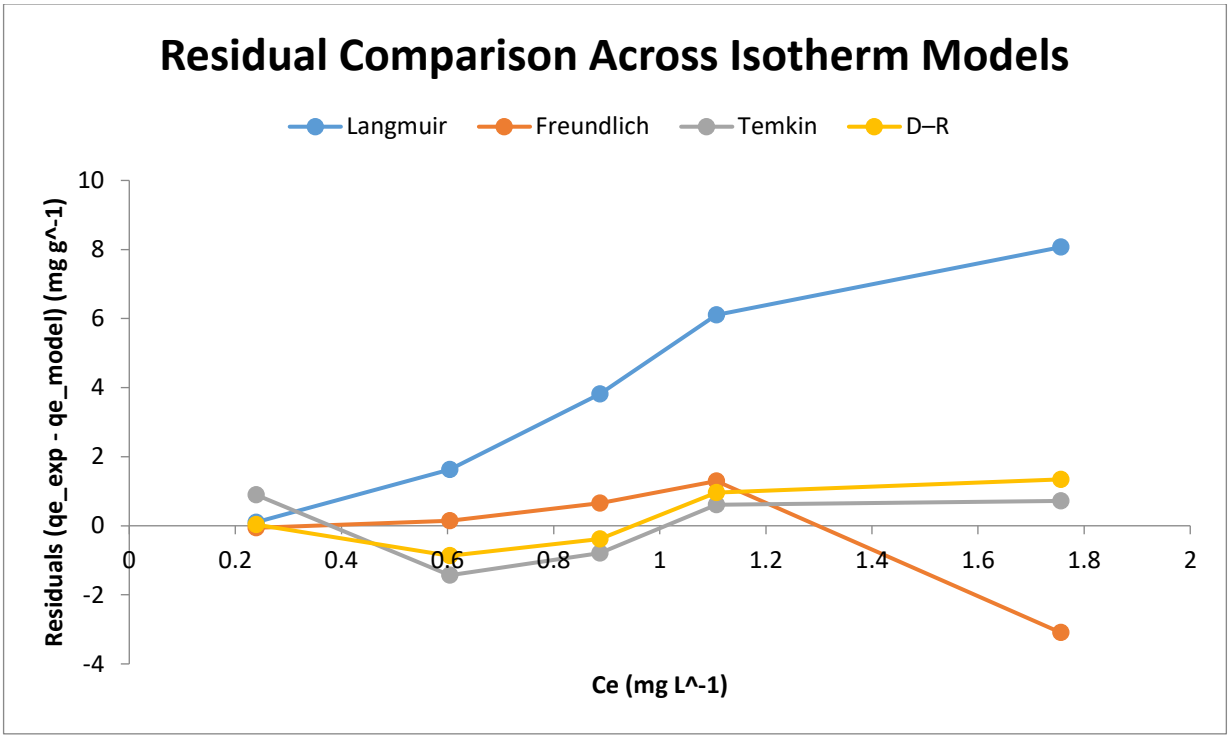

Figure 8: Comparison of residual plots of experimental and modeled adsorption data of Cr(VI) removal by Langmuir, Freundlich, Temkin and Dubinin-Radushkevich isotherm models.

The **Langmuir model** is based on the notion of a monolayer chemisorption of Cr(VI) on a structurally homogeneous adsorbent and it fitted best among the models, showing a high determination constant ($R^2 = 0.9752$) value. A defined straight line was displayed by the Langmuir equation's linear form ($1/q_e$ vs $1/C_e$), indicating that the sorbent's capacity to hold the sorbate is limited.

$$Q_e = Q_L K_L \, C_e \, (1 + K_L C_e)^{-1}$$

The above given Langmuir equation uses the following terms: K_L for Langmuir adsorption constant (L g^{-1}), Q_L stands for the maximum sorbed Cr(VI) (mg g-1), Q_e for number of metal ions adsorbed on the sorbent (mg g^{-1}) at equilibrium, and C_e for the equilibrium concentration of metal ions (mg L^{-1}). According to the Langmuir model, the separation factor (R_L) explains that the sorption of Cr(VI) by nano-ferrihydrite is favorable. The value of R_L was less than one, which shows Cr(VI) sorption was favorable.

The **Freundlich model** explains the sorption occurring on one or more layers or heterogeneous sorption surface ($R^2 = 0.9729$). This is illustrated in the equation below.

$$q_e = K_F C_e^{\,1/n}$$

K_F is the relative sorption capacity of Cr(VI) ($mg^{1-n}\ g^{-1}$ ln) and n shows linearity. The adsorption intensity is represented by the heterogeneity factor, 1/n. The n value was 0.5, indicating moderate surface heterogeneity (Lesaoana, 2018) and the Freundlich constant (K_F) was 4.77, further validating the suitability of nano-ferrihydrite as an efficient sorbent for Cr(VI). The plot of $\log q_e$ versus $\log C_e$ yielded a linear relationship, signifying the applicability of the model.

The **Temkin isotherm model**, which considers adsorbent–adsorbate interactions, provided a reasonable fit with an R^2 value of 0.9118. The linear plot of Q_e versus $\ln C_e$ suggests that the adsorption energy is reduced linearly with the coverage of the sorbent surface and is described as:

$$Q_e = RT/(AC_e)$$

Here, the universal gas constant is R, T is the absolute temperature, b is the sorption heat and is an important parameter that distinguishes the sorbent efficacy for sorption and A is the binding constant (Samir *et al*., 2019).

The **Dubinin–Radushkevich (D–R) isotherm model**, known for its capacity to distinguish between physical and chemical adsorption. The plot of ln q_e versus ε^2 indicated a high correlation ($R^2 = 0.9734$), suggesting a chemisorption-driven mechanism or potential pore-filling behavior. The model is represented below:

$$Q_e = Q_D\ (-[RTIn(1 + 1/C_e)]^2)$$

Q_D is the adsorption capacity (mg g^{-1}) and B_D is the mean free energy of sorption. For the Dubinin-Radushkevich model, the (E) bonding energy was also determined to be < 8, indicating that the dominant process could be physical sorption (Mudhoo and Pittman, 2023).

Overall, the Langmuir and D–R models demonstrated the highest correlation coefficients, indicating that Cr(VI) sorption onto nano-ferrihydrite is primarily governed by monolayer coverage on a relatively uniform surface and may involve chemisorption mechanisms. The results also confirm the complexity of the adsorption system, where multiple processes such as surface heterogeneity, energy distribution, and potential multilayer formation contribute to the overall removal efficiency.

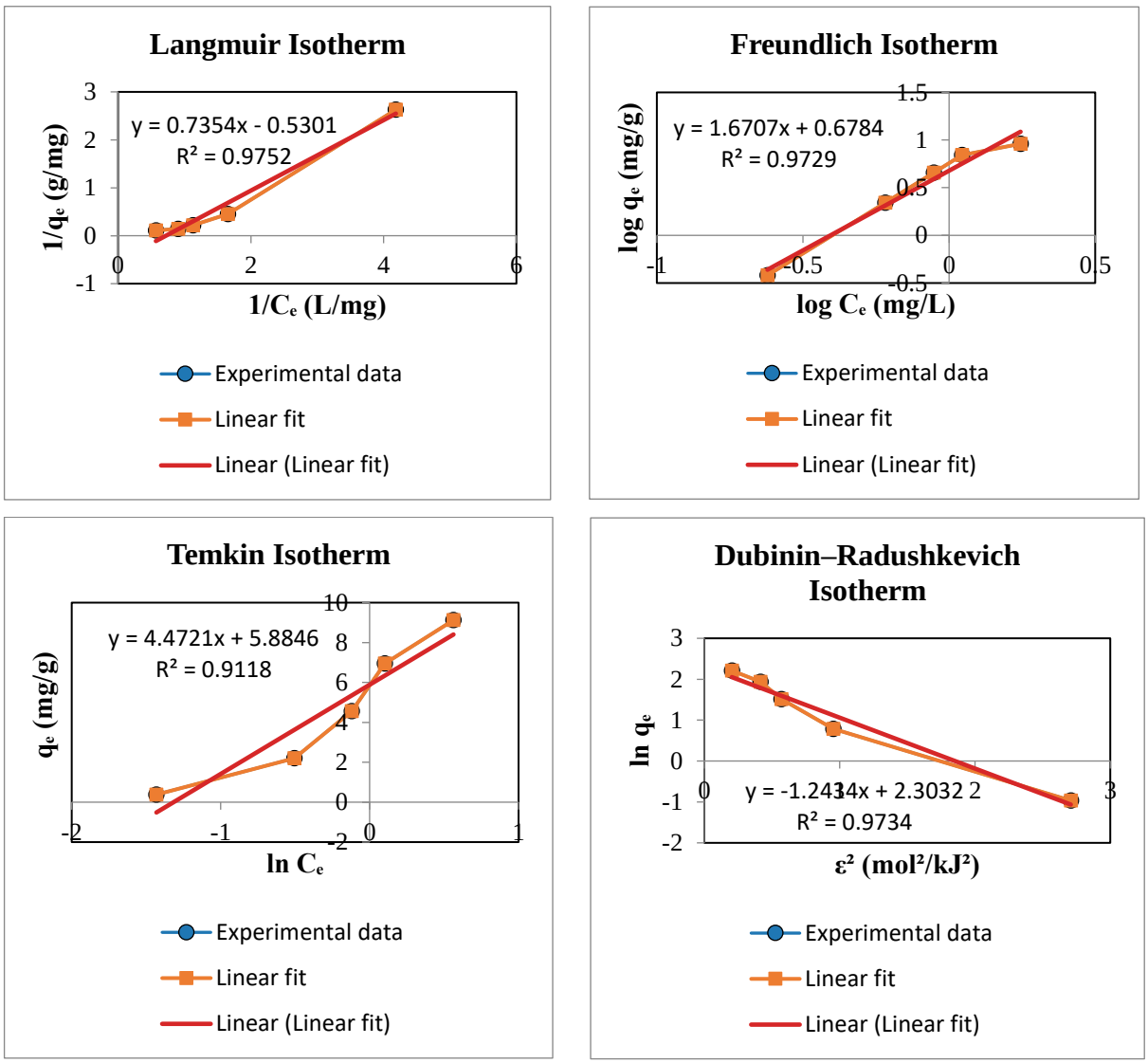

Figure 9: Cr(VI) sorption isotherms by nano-ferrihydrite at pH 2-10, temperature 25 ° C and a dose of sorbent 2 gL^{-1}. The straight line (——) reflects the experimental observations, the model suits and block circle (°) show observational evidence.

Table 2: Non-linear model parameters for the sorption of Cr(VI) onto nano-ferrihydrite at a sorbent dosage of 2 gL^{-1}, an initial concentration of 0–20 mgL^{-1}, and a temperature of 25 °C.

Sorbent	**Langmuir**			**Freundlich**			**Temkin**			**Dubinin-Redushkevich**		
	QL (mg g^{-1})	**KL (L g^{-1})**	**R^2**	**QF (mg $^{1-n}$ g^{-1} Ln)**	**1/n**	**R^2**	**B**	**A**	**R^2**	**QD (mg g^{-1})**	**E (kJ g^{-1})**	**R^2**
Nano-ferrihydrite	1.88	0.72	0.975	0.59	1.67	0.972	554.07	3.72	0.912	10.006	1.57	0.973

3.6. Fourier transform infrared spectra of nano-ferrihydrite

To investigate the chemical composition of the material, molecules are subjected to infrared radiation in FTIR spectroscopy. Metal chemical bonds stretch, shrink, and bend when exposed to infrared light. The spectrum's chemical functional group begins to absorb infrared light at a specific wavelength range, independent of the molecule's overall structure (Khan *et al*., 2018). Spectra were captured between 1000 to 3500 cm^{-1}. FTIR spectra obtained for this analysis indicated the presence of functional groups on the surface of the sorbent with and without Cr(VI) loading. FTIR spectra peaks shifted, disappeared and new peaks appeared. To determine which functional groups in nano-ferrihydrite are the cause of metal sorption, FTIR analysis was performed on the solid phase (Figure 10).

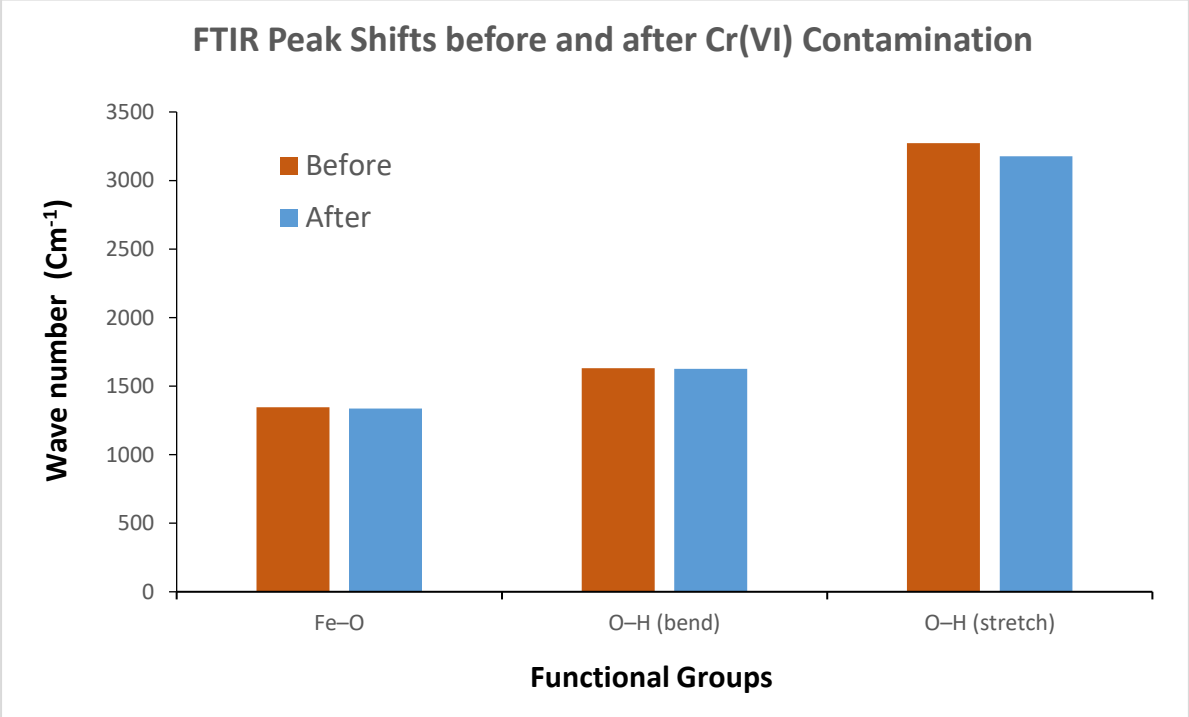

Figure 10: FTIR peak shifts before and after adsorption show the variation in functional group wavenumber for Cr(VI) sorption

The FTIR spectra of nano-ferrihydrite show some adsorption peaks for different functional groups, suggesting its complex nature with a metallic species affinity. In Figure 11, the nano-ferrihydrite spectra before Cr (VI) interaction are depicted. The peak at 1346 cm^{-1} appearing in the spectra of nano-ferrihydrite is identified as the Fe-O group fingerprint, which helps in redox reactions to reduce Cr(VI) to Cr(III). The peaks at 1632 and 3272 cm^{-1} are due to the O-H functional, which strengthens metal binding through hydrogen bonding and surface complexation (Fotodimas *et al*., 2024).

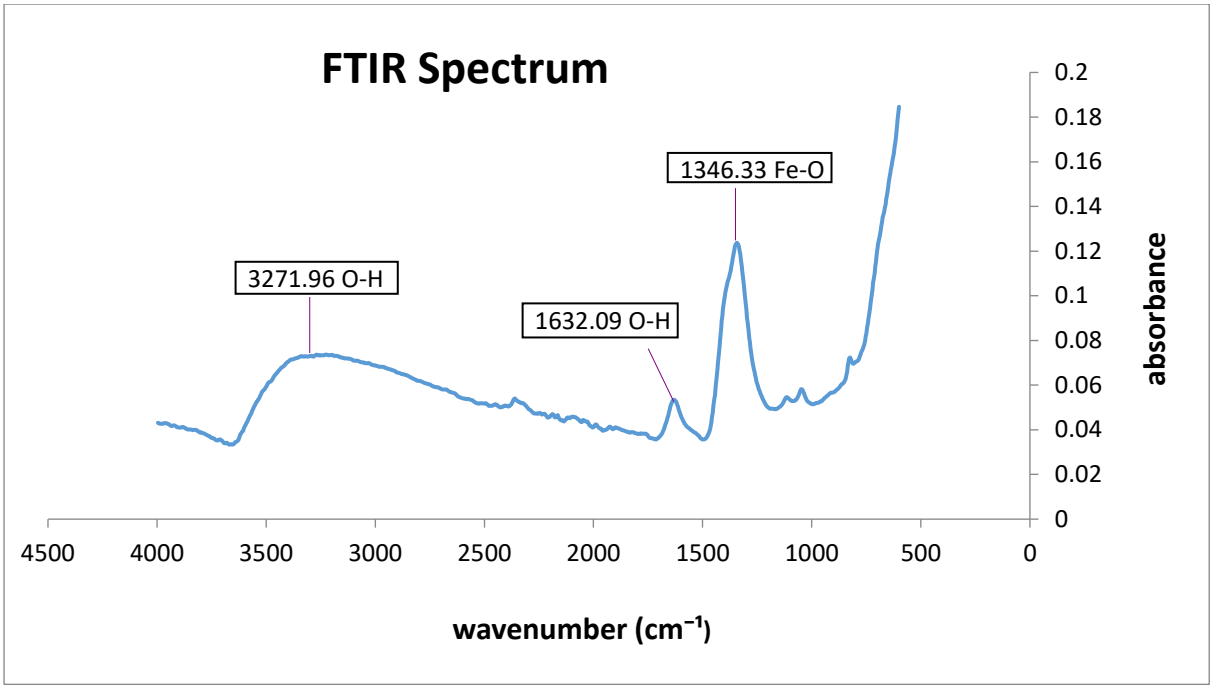

Figure 11: FTIR spectrum of uncontaminated nano-ferrihydrite

Figure 12 shows the spectra of nano-ferrihydrite after the interaction with Cr(VI). After interacting with Cr(VI), variations in peaks were observed. Peak at 1346 cm^{-1} in unloaded sorbent moved to 1336 cm^{-1} in metal-loaded spectra due to the interaction of Fe-O with metal. The peaks observed at 1632 and 3272 cm^{-1} shifted to 1627 and 3177 $cm^{-1,}$ showing the involvement of the O-H functional group in metal sorption from contaminated water. FTIR spectra revealed that the hydroxyl group plays a key role in chromate adsorption, as indicated by the variation in the peak after chromate adsorption (Zhan *et al.*, 2020). Some spectra's absorption peaks were same, suggesting that surface functional groups were mostly unchanged during the composites' production and interaction with Cr (VI). However, the surface functional groups' peak intensities dropped following the reaction, indicating that they actively contributed to the elimination of Cr (VI). The shift in peaks after contamination of Cr(VI) showed the redox transformation of Cr(VI), which supports environmental remediation.

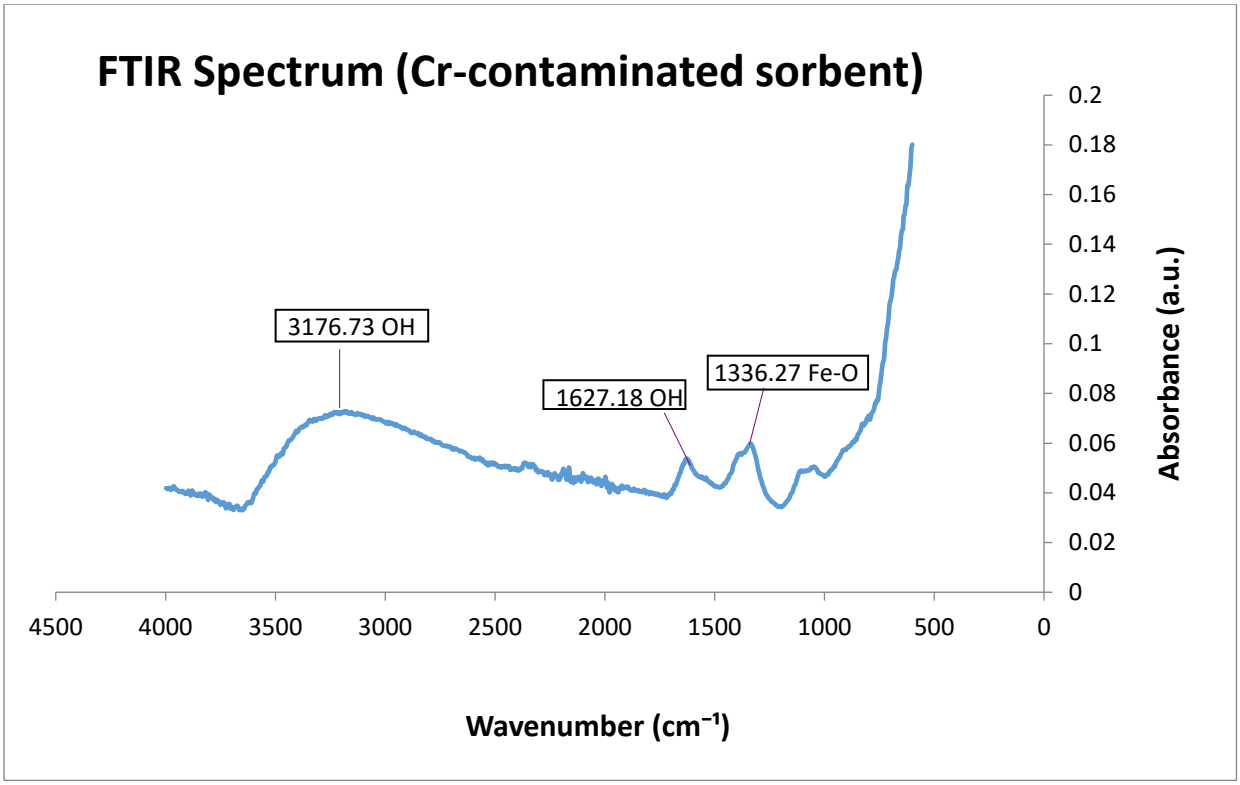

Figure 12: FTIR spectrum of Cr(VI) contaminated nano-ferrihydrite

4. Conclusion

This study investigated the potential of nano-ferrihydrite that was synthesized in the laboratory to remove Cr(VI) from contaminated water due to its cheap and eco-friendly nature. Batch studies were carried out to assess the effect of several factors on their efficiencies for Cr(VI) removal. The factors included pH, initial Cr(VI) concentration, sorbent dose and contact time. At pH 3, there was 92% Cr(VI) sorption efficiency at the initial concentration of 15 mg L^{-1}, 2 h contact time and 2 gL^{-1} sorbents. The nano-ferrihydrite attained maximum sorption of 93 % at 8 hours of contact time, while maximum sorption (92%) was observed at 15 mgL-1 Cr(VI) concentration. The highest sorption rate (92.5%) was achieved using a 4 gL-1 sorbent dose. The data collected matched both Langmuir and D-R isotherm and second-order models, indicating that chemo-sorption is the main method to remove Cr(VI) from contaminated water. FTIR analysis showed that nano-ferrihydrite was mainly responsible for chromate adsorption through surface functional groups, whereas chromate sorption was specifically influenced by hydroxyl groups. When sorbents can be reused, an extra economic advantage is attained, along with better environmental performance. The Cr(VI) sorption capacity of nano-ferrihydrite in a column system should be investigated for future large-scale applications.

5. References

1. Abuzarova, K., and Korchuganova, O. (2020, April). Nanosized iron oxyhydroxide: properties, application, preparation. In Journal of Physics: Conference Series (Vol. 1534, No. 1, p. 012002). IOP Publishing.
2. Afzaal, M., Hameed, S., Liaqat, I., Ali Khan, A. A., Abdul Manan, H., Shahid, R., and Altaf, M. (2022). Heavy metal contamination in water, sediments and fish of freshwater ecosystems in Pakistan. Water Practice & Technology, 17(5), 1253-1272.
3. Ahmed, M., S. Ali, S. El-Dek and A. Galal. 2013. Magnetite–hematite nanoparticles prepared by green methods for heavy metal ions removal from water. Mater. Sci. Eng. 178:744-751.
4. Ali, I.H., M.K. Al Mesfer, M.I. Khan, M. Danish and M.M. Alghamdi. 2019. Exploring the adsorption process of lead(II) and chromium(VI) ions from aqueous solutions on acid-activated carbon prepared from Juniperus procera leaves. Processes. 7:217-225.
5. Almeida, J.C., C.E. Cardoso, D.S. Tavares, R. Freitas, T. Trindade, C. Vale and E. Pereira. 2019. Chromium removal from contaminated waters using nanomaterials–a review. Trends. Analyt. Chem. 118:277-291.
6. Al-Sabagh, A., Y. Moustafa, A. Hamdy, H. Killa, R. Ghanem and R. Morsi. 2018. Preparation and characterization of sulfonated polystyrene/magnetite nanocomposites for organic dye adsorption. Egypt. J. Pet. 27:403-413.
7. Alsuhaibani, A. M., Alayyafi, A. A., Albedair, L. A., El-Desouky, M. G., and El-Bindary, A. A. (2024). Efficient fabrication of a composite sponge for Cr (VI) removal via citric acid cross-linking of metal-organic framework and chitosan: adsorption isotherm, kinetic studies, and optimization using Box-Behnken design. Materials Today Sustainability, 26, 100732.
8. Barletta, M., A.R. Lima and M.F. Costa. 2019. Distribution, sources and consequences of nutrients, persistent organic pollutants, metals and microplastics in south American estuaries. Sci. Total Environ. 651:1199-1218.
9. Baskar, A. V., Bolan, N., Hoang, S. A., Sooriyakumar, P., Kumar, M., Singh, L., and Siddique, K. H. (2022). Recovery, regeneration and sustainable management of spent adsorbents from wastewater treatment streams: A review. Science of the Total Environment, 822, 153555.

10. Binabaj, M.A., S. Nowee and N. Ramezanian. 2018. Comparative study on adsorption of Cr(VI) from industrial wastewater onto nature-derived adsorbents (brown coal and zeolite). Int. J. Environ. Sci. Technol. 15:1509-1520.
11. Borna, M.O., M. Pirsaheb, M.V. Niri, R.K. Mashizie, B. Kakavandi, M.R. Zare and A. Asadi. 2016. Batch and column studies for the adsorption of chromium(VI) on low-cost hibiscus cannabinus kenaf, a green adsorbent. J. Taiwan Inst. Chem. Eng. 68:80- 89.
12. Cao, Y., Dong, S., Dai, Z., Zhu, L., Xiao, T., Zhang, X., and Soltanian, M. R. (2021). Adsorption model identification for chromium (VI) transport in unconsolidated sediments. Journal of Hydrology, 598, 126228.
13. Chakraborty, R., Asthana, A., Singh, A. K., Jain, B., and Susan, A. B. H. (2022). Adsorption of heavy metal ions by various low-cost adsorbents: a review. International Journal of Environmental Analytical Chemistry, 102(2), 342-379.
14. Chakraborty, R., Verma, R., Asthana, A., Vidya, S. S., and Singh, A. K. (2021). Adsorption of hazardous chromium (VI) ions from aqueous solutions using modified sawdust: kinetics, isotherm and thermodynamic modelling. International Journal of Environmental Analytical Chemistry, 101(7), 911-928.
15. Chen, Z., D. Wei, Q. Li, X. Wang, S. Yu, L. Liu, B. Liu, S. Xie, J. Wang and D. Chen. 2018. Macroscopic and microscopic investigation of Cr(VI) immobilization by nanoscaled zero-valent iron supported zeolite mcm-41 via batch, visual, XPS and EXAFS techniques. J. Clean. Prod. 181:745-752.
16. Chrysochoou, M. and A. Ting. 2011. A kinetic study of Cr(VI) reduction by calcium polysulfide. Sci. Total Environ. 409:4072-4077.
17. DeFilippi, L. J. (2018). Bioremediation of hexavalent chromium in water, soil, and slag using sulfate-reducing bacteria. In Remediation of hazardous waste contaminated soils (pp. 437-457). Routledge.
18. Di Baldassarre, G., M. Sivapalan, M. Rusca, C. Cudennec, M. Garcia, H. Kreibich, M. Konar, E. Mondino, J. Mård and S. Pande. 2019. Sociohydrology: Scientific challenges in addressing the sustainable development goals. Water Resour. Res. 55:6327-6355.

19. Felipe, E. C. B., Batista, K. A., and Ladeira, A. C. Q. (2021). Recovery of rare earth elements from acid mine drainage by ion exchange. Environmental Technology, 42(17), 2721-2732.
20. Fenti, A., Chianese, S., Iovino, P., Musmarra, D., and Salvestrini, S. (2020). Cr (VI) sorption from aqueous solution: a review. Applied Sciences, 10(18), 6477.
21. Fotodimas, I., Ioannou, Z., Kanlis, G., Sarris, D., and Athanasekou, C. (2024). Sustainable Management of Shrimp Waste to Produce High-Added Value Carbonaceous Adsorbents. Sustainability, 16(23), 10305.
22. Georgaki, M. N., Charalambous, M., Kazakis, N., Talias, M. A., Georgakis, C., Papamitsou, T., and Mytiglaki, C. (2023). Chromium in water and carcinogenic human health risk. Environments, 10(2), 33.
23. Guo, X., Liu, A., Lu, J., Niu, X., Jiang, M., Ma, Y., and Li, M. (2020). Adsorption mechanism of hexavalent chromium on biochar: kinetic, thermodynamic, and characterization studies. ACS omega, 5(42), 27323-27331.
24. Hassan, A. I., and Saleh, H. M. (2022). Toxicity and hazardous waste regulations. In Hazardous Waste Management (pp. 165-182). Elsevier.
25. Hiemstra, T., Hofmann, A., Mendez, J. C., and Bai, Y. (2024). Surface complexation and reactivity of ferrihydrite in relation to its surface and mineral structure, with applications to natural systems. Reviews in Mineralogy and Geochemistry, 91(1), 175-227.
26. Hosseini, S. G., and Pasikhani, J. V. (2019). Kinetic and thermodynamic investigation on the adsorption of hexavalent chromium pollution by Fe3O4/AC/TiO2 nanotubes as a novel ternary magnetic nanocomposite. Desalination and Water Treatment, 152, 351-365.
27. Hu, X., Ding, Z., Zimmerman, A. R., Wang, S., and Gao, B. (2015). Batch and column sorption of arsenic onto iron-impregnated biochar synthesized through hydrolysis. Water research, 68, 206-216.
28. Islam, M. A., Angove, M. J., and Morton, D. W. (2019). Recent innovative research on the chromium (VI) adsorption mechanism. Environmental Nanotechnology, Monitoring & Management, 12, 100267.
29. Itankar, N., and Patil, Y. (2022). Assessing physicochemical technologies for removing hexavalent chromium from contaminated waters-An overview and future research directions. Water, Air, & Soil Pollution, 233(9), 355.

30. Jerin, V., R. Remya, M. Thomas and J.T. Varkey. 2019. Investigation of the removal of toxic chromium ions from wastewater using Fe2O3 nanoparticles. Mater. Today: Proc. 9:27-31.
31. Jan, A., Hussain, Z., Ullah, A., Ahmed, Z., Bakhsh, B. P., Latif, A., ... & Ahmed, M. (2025). Sugarcane Whip Smut: A Comprehensive Review of Pathogen Biology, Epidemiology, and Control Measures. *Annual Methodological Archive Research Review*, *3*(5), 211-232.
32. Jan, A., Shaikh, G. Y., Ullah, S., Saddam, S., Ali, T., u Rehman, A., ... & Ahmed, M. (2025). In-vitro antifungal activity of medicinal plant extracts against Fusarium oxysporum causing wilt in okra. *Indus Journal of Bioscience Research*, *3*(8), 406-414.
33. Jan, A., Adil, S., Ali, T., Ahmed, B., Ahmed, Z., & Hussain, Z. (2025). Desert and medicinal plants as novel sources of antimicrobial agents for crop protection. *Planta Animalia*, *4*(3), 197-218.
34. Jan, A., Ali, T., Chirag, S., Ahmed, S., Ali, M., Wali, S., ... & Ullah, K. (2025). Eco-Friendly Management of Insect Pests and Plant Diseases Using Botanical Extracts. *Global Research Journal of Natural Science and Technology*.
35. Jan, A., Razzaq, F., Umair, M., Ullah, I., Shamsullah, S., Uzair, M., Ikram, M., Ayyaz, M., & Ali, T. (2025). Cotton Leaf Curl Disease: Pathogen Diversity, Whitefly Ecology, and Integrated Management Approaches. *Planta Animalia*, *4*(4), 363-371.
36. Khalil, U., M.B. Shakoor, S. Ali, M. Rizwan, M.N. Alyemeni and L. Wijaya. 2020. Adsorption-reduction performance of tea waste and rice husk biochars for Cr(VI) elimination from wastewater. J. Saudi Chem. Soc. 24:799-810.
37. Khan, S. A., Khan, S. B., Khan, L. U., Farooq, A., Akhtar, K., and Asiri, A. M. (2018). Fourier transform infrared spectroscopy: fundamentals and application in functional groups and nanomaterials characterization. Handbook of materials characterization, 317-344.
38. Kokab, T., Ashraf, H. S., Shakoor, M. B., Jilani, A., Ahmad, S. R., Majid, M., and Hakeem, K. R. (2021). Effective removal of Cr (Vi) from wastewater using biochar derived from walnut shell. International Journal of Environmental Research and Public Health, 18(18), 9670.
39. Kong, X., Z. Han, W. Zhang, L. Song and H. Li. 2016. Synthesis of zeolite-supported microscale zero-valent iron for the removal of Cr(VI) and Cd(II) from aqueous solution. J. Environ. Manage. 169:84-90.
40. Kucic, D., M. Simonič and L. Furač. 2017. Batch adsorption of Cr (VI) ions on zeolite and agroindustrial waste. Chem. Biochem. Eng. Q. 31:497-507.
41. Lace, A., D. Ryan, M. Bowkett and J. Cleary. 2019. Chromium monitoring in water by colorimetry using optimized 1, 5-diphenyl carbazide method. Intern. J. Environ. Res. Public Health. 16:1803-1810.

42. Lesaoana, M. (2018). Simultaneous sequestration of Cr (VI) and Cr (III) from aqueous solutions by activated carbon and ion-imprinted polymers (Master's thesis, Vaal University of Technology (South Africa)).
43. Liang, C., Wu, H., Chen, J., and Wei, Y. (2023). Mechanistic insights into the interfacial adsorption behaviors of Cr (VI) on ferrihydrite: effects of pH and naturally coexisting anions in the environment. Ecotoxicology and Environmental Safety, 249, 114474.
44. Lin, H., Wang, Z., Liu, C., and Dong, Y. (2022). Technologies for removing heavy metal from contaminated soils on farmland: A review. Chemosphere, 305, 135457.
45. Liu, R., Chi, L., Wang, X., Wang, Y., Sui, Y., Xie, T., and Arandiyan, H. (2019). Effective and selective adsorption of phosphate from aqueous solution via trivalent-metals-based amino-MIL-101 MOFs. Chemical Engineering Journal, 357, 159-168.
46. Masindi, V. and K.L. Muedi. 2018. Environmental contamination by heavy metals. Heavy Metals. 10:115-132.
47. Masood ul Hasan, I., Javed, H., Hussain, M. M., Shakoor, M. B., Bibi, I., Shahid, M., and Niazi, N. K. (2023). Biochar/nano-zerovalent zinc-based materials for arsenic removal from contaminated water. International journal of phytoremediation, 25(9), 1155-1164.
48. Mudhoo, A., and Pittman Jr, C. U. (2023). The Dubinin-Radushkevich models: Dissecting the ps/p to cs/ce replacement in solid-aqueous interfacial adsorption and tracking the validity of E= 8 kJ mol–1 for assigning sorption type. Chemical Engineering Research and Design, 198, 370-402.
49. Nieder, R., D.K. Benbi and F.X. Reichl. 2018. Soil-borne particles and their impact on the environment and human health. In Soil components and human health: Springer. 22:99-177.
50. Owalude, S.O. and A.C. Tella. 2016. Removal of hexavalent chromium from aqueous solutions by adsorption on modified groundnut hull. BJBAS. 5:377-388.
51. Ragadhita, R. I. S. T. I., and Nandiyanto, A. B. D. (2022). Curcumin adsorption on zinc imidazole framework-8 particles: Isotherm adsorption using Langmuir, Freundlich, Temkin, and Dubinin-Radushkevich models. J. Eng. Sci. Technol, 17(2), 1078-1089.

52. S. Ali, N.S. Bolan and Y.S. Ok. 2016. Remediation of arsenic-contaminated water using agricultural wastes as biosorbents. Crit. Rev. Environ. Sci. Technol. 46:467- 499.
53. Samir, L., Samira, A., Mekatel, E. H., and Djamel, N. (2019). Adsorption of Cr (VI) on Stipa tenacissima L (Alfa): Characteristics, kinetics and thermodynamic studies. Separation Science and Technology, 54(6), 876-887.
54. Shin, S. S., Jung, Y., Jeon, S., Park, S. J., Yoon, S. J., Jung, K. W., and Lee, J. H. (2024). Efficient recovery and recycling/upcycling of precious metals using hydrazide-functionalized star-shaped polymers. Nature communications, 15(1), 3889.
55. Tafakori, V., R. Zadmard, F. Tabandeh, M.A. Amoozegar and G. Ahmadian. 2017. Equilibrium isotherm, kinetic modeling, optimization and characterization studies of cadmium adsorption by surface-engineered Escherichia coli. Iran. Biomed. J. 21:380- 388.
56. Tiadi, N., M. Mohanty, C. Mohanty and H.P. H. Panda. 2017. Studies on the adsorption behavior of industrial waste for the removal of chromium from aqueous solution. S. Afr. J. Chem. Eng. 23:132-138.
57. Wang, Y., Y. Li, H. Li, H. Zheng and Q. Du. 2019. Equilibrium, kinetic and thermodynamic studies on methylene blue adsorption by konjac glucomannan/activated carbon aerogel. J. Polym. Environ. 27:1342-1351.
58. Xu, J., Liu, M., Ma, G., Zheng, D., Zhang, X., and Hou, Y. (2023). Valuable recovery technology and resource utilization of chromium-containing metallurgical dust and slag: a review. Metals, 13(10), 1768.
59. Yu, L.J., S.S. Shukla, K.L. Dorris, A. Shukla and J. Margrave. 2008. Adsorption of chromium from aqueous solutions by maple sawdust. J. Hazard. Mater. 100:53-63.
60. Yusuff, A.S. 2019. Adsorption of hexavalent chromium from aqueous solution by Leucaena leucocephala seed pod activated carbon: Equilibrium, kinetic and thermodynamic studies. Arab J. Basic Appl. Sci. 26:89-102.
61. Zhan, G., Li, J., Hu, Y., Zhao, S., Cao, S., Jia, F., and Zhang, L. (2020). The surface hydroxyl and oxygen vacancy dependent Cr (VI) adsorption performance of BiOCl. Environmental Science: Nano, 7(5), 1454-1463.
62. Zhang, J., Yang, H. B., Zhou, D., and Liu, B. (2022). Adsorption energy in oxygen electrocatalysis. Chemical Reviews, 122(23), 17028-17072.

63. Zhang, L., F. Fu, G. Yu, G. Sun and B. Tang. 2022. The fate of Cr(VI) during aging of ferrihydrite-humic acid co-precipitates: Comparative studies of structurally incorporated Al(III) and Mn(II). Sci.Total Environ. 807:151073-151081.
64. Zhao, Z., H. An, J. Lin, M. Feng, V. Murugadoss, T. Ding, H. Liu, Q. Shao, X. Mai and N. Wang. 2019. Progress on the photocatalytic reduction removal of chromium contamination. Chem. Rec. 19:873-882.
65. Zoroddu, M. A., Aaseth, J., Crisponi, G., Medici, S., Peana, M., and Nurchi, V. M. (2019). The essential metals for humans: a brief overview. Journal of inorganic biochemistry, 195, 120-129.
66. Ochie, O. S., Okonkwo, S. I., & Okwuego, O. P. (2025). Synthesis and characterization of nanostructured sorbents derived from rice husks using FTIR, SEM, TEM and XRD approaches. *International Research Journal of Pure and Applied Chemistry*, *26*(1), 38-48.
67. Molavi, H., Moghimi, H., & Taheri, R. A. (2020). Zr-based mofs with high drug loading for adsorption removal of anti-cancer drugs: A potential drug storage. *Applied Organometallic Chemistry*, *34*(4), e5549.
68. Perveen, S. (2023). Drinking water quality monitoring, assessment and management in Pakistan: A review. *Heliyon*, *9*(3).
69. Wang, Z., Bi, X., He, X., Xie, Y., Lin, J., & Deng, B. (2023). A two-sorbent system for fast uptake of arsenate from water: Batch and column studies. *Water Research, 228*, 119290.